Lab on a Chip

PAPER

View Article Online
View Journal

Cite this: DOI: 10.1039/c7lc00930e

Persistent drought monitoring using a microfluidic-printed electro-mechanical sensor of stomata *in planta*†

Volodymyr B. Koman,[a] Tedrick T. S. Lew,[a] Min Hao Wong,[a] Seon-Yeong Kwak,[a] Juan P. Giraldo[b] and Michael S. Strano*[a]

Stomatal function can be used effectively to monitor plant hydraulics, photosensitivity, and gas exchange. Current approaches to measure single stomatal aperture, such as mold casting or fluorometric techniques, do not allow real time or persistent monitoring of the stomatal function over timescales relevant for long term plant physiological processes, including vegetative growth and abiotic stress. Herein, we utilize a nanoparticle-based conducting ink that preserves stomatal function to print a highly stable, electrical conductometric sensor actuated by the stomata pore itself, repeatedly and reversibly for over 1 week. This stomatal electro-mechanical pore size sensor (SEMPSS) allows for real-time tracking of the latency of single stomatal opening and closing times *in planta*, which we show vary from 7.0 ± 0.5 to 25.0 ± 0.5 min for the former and from 53.0 ± 0.5 to 45.0 ± 0.5 min for the latter in *Spathiphyllum wallisii*. These values are shown to correlate with the soil water potential and the onset of the wilting response, in quantitative agreement with a dynamic mathematical model of stomatal function. A single stoma of *Spathiphyllum wallisii* is shown to distinguish between incident light intensities (up to 12 mW cm^{-2}) with temporal latency slow as 7.0 ± 0.5 min. Over a seven day period, the latency in opening and closing times are stable throughout the plant diurnal cycle and increase gradually with the onset of drought. The monitoring of stomatal function over long term timescales at single stoma level will improve our understanding of plant physiological responses to environmental factors.

Received 30th August 2017,
Accepted 16th October 2017

DOI: 10.1039/c7lc00930e

rsc.li/loc

Introduction

Water availability is a major limiting factor for plant growth.[1] By 2100 the global water deficit is expected to escalate, increasing the intensity of drought from 1% to 30%.[2] Drought induced by climate change will have a severe impact on agricultural productivity and ecosystem balance.[3] Soil water deficit results in decreased plant water and nutrient content,[4] leading to the turgor pressure loss, inhibition of cell elongation[5] and cell division.[6] As a consequence, plants experience reduced growth,[7] oxidative damage,[8] and photosynthetic complex disassembly.[8] As the earliest and the fastest drought resistance mechanism, plants regulate their transpiration rates through stomata.[9] Hence stomatal aperture may be a promising indicator of plant response to changes in water balance. However, these plant physiological changes can occur over the time scales of days or even years,[10] requiring persistent and real-time sensors. Herrera *et al.* showed that the collective stomatal conductance, measured for multiple stomata, gradually decreases over 16 days under drought conditions.[11] Cheng *et al.* observed progressive proteomic plant responses during drought conditions over 48 hours.[12] Morari *et al.* reported ion concentration changes in maize shoots and roots over 14 days under drought.[13] All the above mentioned measurements are end point and do not address the problem of monitoring stomatal pore size at long timescales and persistently. Herein, we developed an electrical conductimetric sensor capable of real-time measurement of single stomatal aperture, as well as the stomatal opening and closing dynamics in response to external stimuli.

To date, there remains a dearth of methods for measuring single stomatal function *in planta*, and none offer real-time, long term monitoring under natural conditions. Mold impressions from a leaf surface remain a common imaging technique to assess stomatal aperture but are necessarily static.[14] Several stomatal features fall below Abbe's diffraction limit,[15] confounding resolution by microscopy. Indirect methods such as isotopic labelling, gas exchange,[16] fluorometry,[17] and electrochemistry[18] have several limitations,

[a] Department of Chemical Engineering, Massachusetts Institute of Technology, Cambridge, MA, USA. E-mail: strano@mit.edu
[b] Department of Botany and Plant Sciences, University of California, Riverside, CA, USA

† Electronic supplementary information (ESI) available. See DOI: 10.1039/c7lc00930e

preventing real-time, persistent monitoring of a single stomata. While gas exchange measurements provide the collective conductance of multiple stomata,[16] they often require a part of a leaf or an entire plant to be placed in a closed chamber, causing interference with the stomatal natural microenvironment such as removal of the leaf boundary layer. Open chamber alternatives exist, but they either require rigorous environmental control of gas exchange or are very costly.[19] Fluorometric probes can interfere with stomata and photobleach over relatively short periods.[17] Isotopes and electrochemical measurements remain invasive and, thus, limit prolonged measurements.[19]

Developments in flexible and macro-electronics have proven to be successful in placing conducting microcircuits onto human skin tissue.[20] Similarly, Lee *et al.* transferred conducting electrodes onto leaf surface;[21] however, their process involved rinsing with acetone, which often hinders stomata function if not structure.[22] Epidermal electrodes typically do not require specific alignment or orientation. In contrast, the problem of stomata actuation of an topical circuit requires fairly precise positioning across the single stoma pore with dimensions ranging from 5–10 μm. Hot embossing requires high temperatures[23] that can damage leaf tissues;[24] microprinting techniques have difficulties printing micrometer-size drops;[25] while photolithography uses damaging UV irradiation as well as corrosive solvents for photoresist development.[26] Direct printing is difficult because the leaf surface is non-planar with non-uniform wetting properties.[27] Finally, material biocompatibility in this case needs to be redefined so that normal stomatal function is not impaired.

Herein, we develop a stomatal electro-mechanical pore size sensor (SEMPSS) to trace single stoma-aperture dynamics. To this end, biocompatible microcircuits are directly printed onto the leaf using open microfluidic guides that yield printing with micrometer precision. Subsequent electrical resistance monitoring across these electrodes allowed us to assess stomatal opening and closing latencies. In combination with a comprehensive stomatal signaling model, these latencies unveil stomatal dynamics, suggesting an important predictive tool. As an application, we demonstrate how SEMPSS can be used as a living light microdetector, which is sensitive to visible light incident on the wild-type peace lily (*Spathiphyllum wallisii*) leaf. This microdetector can operate on a living leaf for days, monitoring stomatal function diurnal cycles. The sensor captures changes in these cycles during soil water deficit periods, tapping into rich stomatal information previously inaccessible to us and opening new ways for monitoring plant states with single stoma precision.

Methods

Plant material

Wild type *Spathiphyllum wallisii* plants were grown in ambient conditions (22 °C and 20% humidity) under 12 h light cycle (incident intensity 10 mW cm^{-2}, FL-70 W, Sinostar with light spectrum shown in Fig. S11†). A typical pot had a size of 13 cm in diameter and 15 cm in height. Unless otherwise stated, plants were well-watered. Water was added as specified directly to the soil in 150 ml aliquots. All experiments were performed at ambient conditions (22 °C and 20% humidity). Specimens were typically 25 cm in diameter and 30 cm in height. Soil water potential was measured using an irrometer (T206, Frostproof).

Illumination and optical stomatal aperture measurements

Optical stomatal aperture measurements were performed using an inverted microscope Zeiss Observer Z1. We used one lamp (FL-70 W, Sinostar) for the red illumination and another lamp (M455 L3, Thorlabs) for blue light illumination (Fig. S11†). A white light lamp included both red and blue parts of spectrum (HAL100, Zeiss). For stomata responsivity experiments, a supercontinuum source (EXW-12, NKT Photonics) and violet lamp (M455 L3, Thorlabs) with a tunable laser filter (LLTF CONTRAST-SR-VIS-HP8, Photon Inc) were used. Light intensity was measured close to the leaf surface using a power meter (PMD100, Thorlabs). All illuminations experiments were performed in a 0.5 × 0.5 × 0.5 m^3 carton box. Unless stated otherwise, the whole plant was illuminated. Partial leaf illumination was achieved using various optical objectives. To optically track the stomatal aperture without interference, short exposure pictures (20 ms) were taken. Optical height profiles were measured by an optical profilorometer (CCI HD, Taylor Hobson).

The measurement error for stomatal aperture obtained from optical microscopy is calculated as the sum of two errors: the standard deviation between different stomata with n indicating the number of stomata compared and measurement error caused by microscope diffraction limit (taken to be 0.3 μm for 100× EC Epiplan Zeiss objective with NA = 0.8).

Electrical measurements

Electrical resistance maps and resistance ink measurements on the leaf surface were performed in the ARS PSF-10-1-4 Cryogenic probe station using micromanipulators as probes (7X, Micromanipulator). Continuous resistance measurements were performed with Keithley 2002 controlled by a home-made LabView interface.

Raman measurements

Raman measurements were performed using 780 nm laser with HR-800 (Horiba BY).

Microfabrication

Microfluidic chips (100 μm long, 100 μm high and 10 μm wide channel; two 3 mm circles for contact pads) for patterning conductive electrodes were fabricated using standard

photolithography techniques. Briefly, photolithographic structures were fabricated using SU-8 photoresist. PDMS (1 : 10 ratio of agent and crosslinking agent) was dropcasted onto the SU-8 structures and cured overnight at 60 °C. Similarly micropillars were fabricated from SU-8 photoresist on 300 nm SiO_2/Si substrates.

A stoma sensor assembly

Spathiphyllum wallisii was selected for method development because of its large stomata.[28] To overcome the limitation presented by the non-planarity of the leaf surface (Fig. S3 and S4†), a layer of soft skin silicone elastomer (Dow corning,

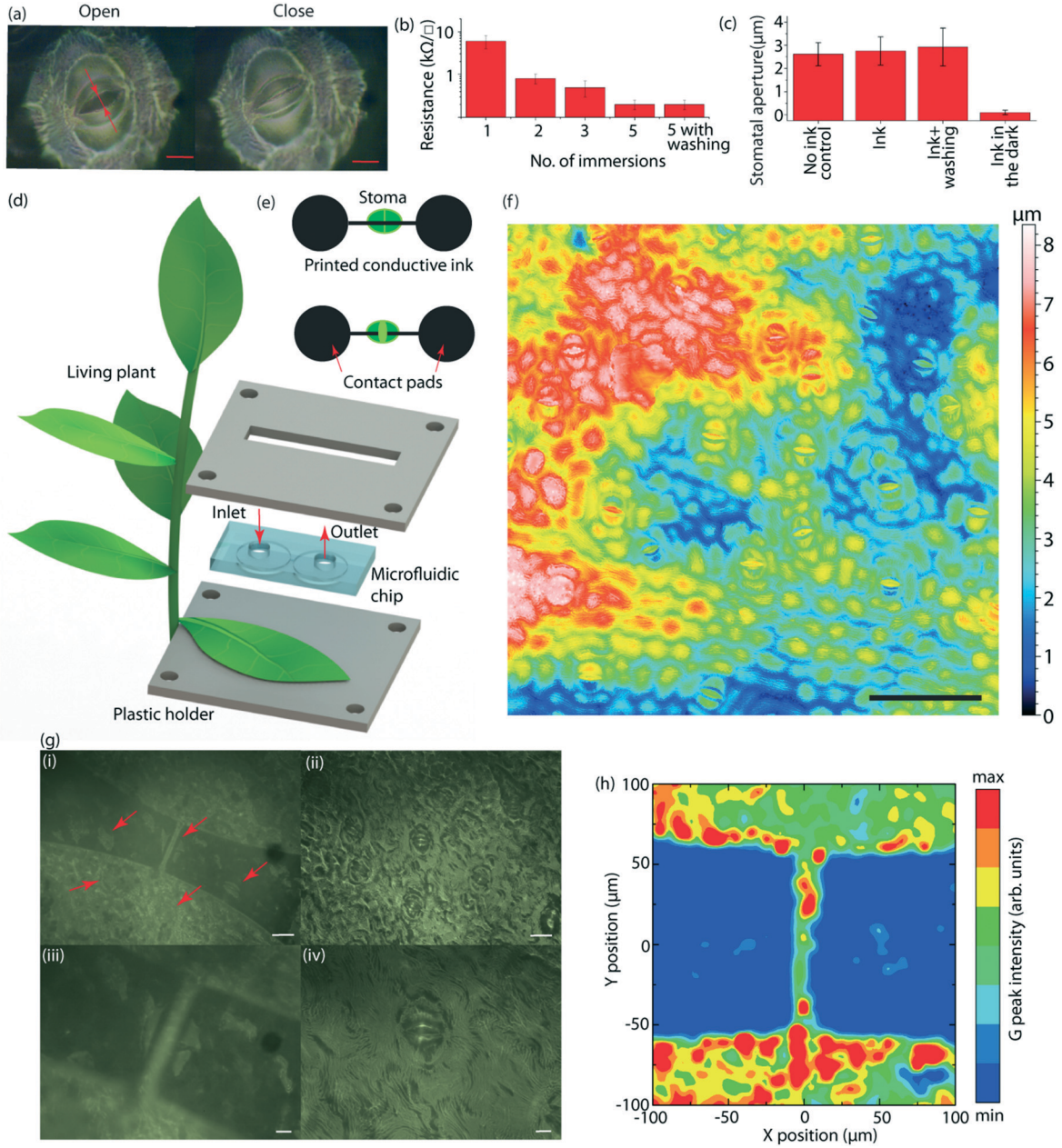

Fig. 1 Printing conductive circuits on *Spathiphyllum wallisii* leaf lamina. (a) Microscope pictures of a stoma in the opened and closed states with the stomatal aperture indicated. Scale bar: 10 μm. (b) Leaf surface resistance after leaf immersion into the conductive ink (n = 10). Bare leaf has ~1 MΩ resistance. (c) Change in stomata sizes after 1 h white light illumination (I = 7 mW cm^{-2}, n = 10), demonstrating that the ink has no effect on the stomatal aperture. (d) Schematics of conductive circuits printing on the leaf surface. A microfluidic chip is placed on top of the leaf abaxial surface and clamped in between two holders. (e) Schematic layout of printed microsensor having two contact pads and a stripe going across a single stoma. Conductive stripe breaks when stoma opens (bottom), increasing sensor resistance. (f) A height profile map demonstrates highly non-planar leaf surface. Scale bar: 75 μm. (g) Bright-field microscopy images of a microfluidic chip aligned on top of a single stoma (i, iii) and the same stoma after printing (ii, iv). Scale bars: 30 μm (i, ii) and 10 μm (iii, iv). Red arrows point to individual stomata. (h) Raman map for carbon nanotube G peak intensity (1590 cm^{-1}) on the leaf surface after the ink printing across a single stoma, demonstrating that the printed ink was confined in the microfluidic channel.

soft skin adhesive kit 7-9850) that spontaneously crosslinks was spincoated on top of the microfluidic chip (60 s, 3000 rpm). To ensure that the microfluidic chip does not become filled with the elastomer, a strip of paper was inserted into the channel during spincoating and removed afterwards. The microfluidic chip was placed on top of the abaxial surface of the leaf kept in the dark. A channel (10 μm thickness) was aligned with a single stoma on the abaxial side of a leaf through a trial-and-error method under the microscope (Fig. S2†). PDMS was cleaned using a white tape prior to alignment on the leaf surface. Special care was taken to avoid placing the microfluidic chip on top of the leaf veins. Once good adhesive contact between the leaf and the microfluidic chip was optically confirmed (Fig. S4†) using long-working distance objective (EC Epiplan-Neofluar 50X, Zeiss), the system was clamped in between two 3D-printed platforms with a narrow slit in the middle to allow ink injection into the microfluidic chip. Approximately 1 hour was allowed for the elastomer to spontaneously crosslink. A conductive ink (AC100, Southwest Nanotechnologies) was used as received and injected into the microfluidic chip using a pipette. This printing procedure was performed only with closed stomata to ensure that the ink does not penetrate inside a plant mesophyll. After 2 hours, water was gently injected into the platform to wash out the residual ink. The assembly was left for 3 hours for water to evaporate; the clamp was released afterwards and the microfluidic chip was gently peeled off. The plant was then placed under the light in order for the patterned stoma to open. This was done to ensure that the electrical connection between the guard cells was broken.

Clean room fabricated SU-8 photoresist micropillars were mechanically scrubbed from SiO_2 surface. To make pillars conductive, we then casted a drop of carbon nanotube ink on top. Once the ink naturally evaporated, we transferred conductive micropillars on top of the leaf surface using a drop of water. The cylindrical shape of micropillars was specifically chosen to maximize pillars adhesion to the leaf surface, while minimizing surface contact area between two pillars to avoid their sticking. Finally, micromanipulators were used to align two micropillars on top of guard cells.

A plant biocompatible conducting ink

A stoma is bordered by a pair of asymmetrical guard cells (Fig. 1a). Under illumination, the chloroplast synthesis of organic solutes, activation of proton pumping,[29] and solute uptake in the guard cells[30] translates into an intracellular osmotic pressure rise through a cascade of biochemical signaling reactions resulting in stomata opening.[31] Taking into account stomatal geometry, the design of our electrical circuit is an open circuited, conducting micro-wire across an open stoma. The circuit is closed when the stoma pore closes to a threshold tolerance (Fig. 1e), allowing electrical indication of the open *versus* closed position. The stomatal aperture can hence be monitored in real time *via* electrical resistance measurements. Note that stretchable strain sensors[32] are not optimal for this function, as they necessarily contract the stomata during opening and limit stomatal gas exchange. A conductive ink must not be cytotoxic to plant cells, but in this work, biocompatibility is extended to include non-perturbative operation of the native stomata itself. Many common conductive inks use silver nanoparticles and/or ethanol-based solvents, which demonstrate apparent cytotoxicity[33] and disruption of stomatal motion,[22] respectively.

To circumvent these limitations, we employed a water-based ink with carbon nanotubes and sodium dodecyl sulfate (SDS) as a surfactant (Fig. S1†). When applied to the leaf surface this ink demonstrates sheet resistances down to 0.2 ± 0.05 kΩ/□ (Fig. 1b). This resistance does not change even after washing the leaf with water to remove residual SDS, illustrating strong ink adhesion. There were no observable differences in stomatal aperture behavior between stomata with printed circuitry and those without (Fig. 1c). Furthermore, even internalized carbon nanotubes of this type in the vasculature, cells and plastids, for example, appear to be biocompatible.[34,35]

To pattern conductive circuits on a living leaf surface with micrometer precision, we aligned a specifically designed, open microfluidic chip guided by optical microscopy and used it as a printing mold (Fig. 1d, e, g and S2†). The leaf surface demonstrates non-planar features with typical height variations of several microns across hundreds microns in the lateral direction (Fig. 1f and S3†). An additional elastomer layer between the leaf and the chip proved to be essential in establishing conformal contact and forming a non-leaking channel (see Methods). To confirm ink deposition across the stoma, the vibrational *G*-peak intensity of the carbon nanotube Raman signal was mapped (Fig. 1h, S5†). The Raman peak is limited to a 10 μm-wide region, proving that the printed ink was successfully confined in the microfluidic channel. Similarly, the mapping of electrical resistance demonstrates the presence of a narrow conductive strip across a single stoma (Fig. S6†). These printed electrodes are ultrathin (based on volume calculations resulting in 10 nm thickness), providing conformal, porous (~1% areal density) coverage, which allows for efficient leaf transpiration and transparent properties (>95% transmission across the visible spectrum).

A stoma sensor fabrication and application

We find that in order to make the sensor stable over many cycles, additional conductive micropillars (5 μm height and 5 μm diameter cylinders) can be placed on top of previously patterned stomata guard cells (Fig. 2c and d). These micropillars proved to be essential with this approach because resistive switching was not persistent without them (see ESI† Note S1). A stoma does not close naturally with the same applied pressure or alignment, making it difficult for the thin printed layer to recover its initial resistance value (Fig. 2b). The patterned stoma with embedded micropillars behaves similarly to the reference non-patterned stoma during three

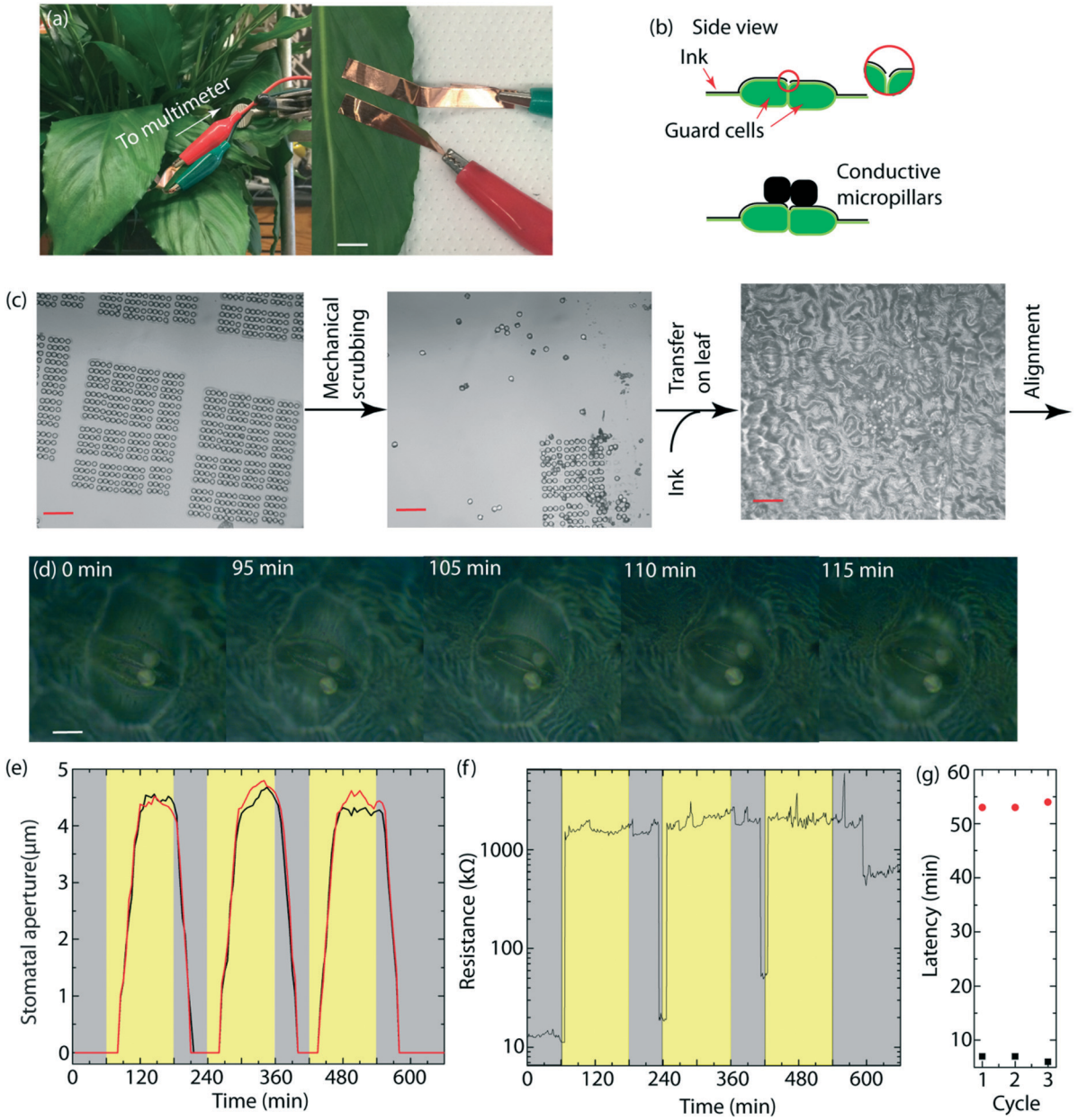

Fig. 2 Application and interface of SEMP sensor. (a) Pictures of a stoma wiring on *Spathiphyllum wallisii*: copper tape is placed directly onto the abaxial leaf surface with a printed ink (left), the wired stoma is connected to a multimeter (right). Scale: 1 cm. (b) Conductive micropillars increase the contact area, improving the electrical contact between two guard cells. Inset shows how the slight variation in stomata closure can lead to the loss of the electrical contact. (c) Optical images of the conductive micropillar transfer on the living leaf. Photolithographically-made micropillars are mechanically scrubbed. Then, a drop of conductive ink (10 μl) is introduced. After water naturally evaporates, micropillars are transferred using drops of water onto the leaf surface where they are further aligned using micromanipulators. Scale bar: 30 μm. (d) Set of microscope images showing two micropillars aligned on top of a stoma. The stoma opens in response to white light illumination (I = 10 mW cm^{-2} starting at t = 60 min). Scale bar: 10 μm. (e) Optically measured stomata aperture dynamics for a patterned stoma with aligned micropillars (black) and a bare stoma (red) in 3 consecutive white light on/off (yellow and grey boxes, respectively) cycles of (I = 10 mW cm^{-2}). Error bars are omitted for clarity. (f) Simultaneous resistance dynamics of the patterned stoma from (d). (g) Stomatal opening (black squares) and closing latency (red circles) for light cycles in (f). Data points have 0.5 min error bars that are not visible.

consecutive on/off light cycles (Fig. 2e, see Methods). Also, polymers have been previously applied on a leaf surface with no effects,[17] and photoresist micropillars, being transparent, should not interfere with photosynthesis.[36]

Once assembled on the surface, the sensor is connected to a multimeter using copper tape (Fig. 2a). The patterned stoma showed repeatable resistance changes in simultaneous electrical measurements, corresponding to on/off contact between micropillars (Fig. 2f). Micropillars lost electrical contact at around 7.0 ± 0.5 min after the light was switched on, henceforth referred to as the opening time latency. The resistance returned to the low state when the stoma closed and

the micropillars regained contact, 53.0 ± 0.5 min after light was switched off, or the closing latency. This demonstrates the ability to electrically sense incident visible light. In comparing the sensor to optical microscopy, we note that it detects the early stages of opening undetectable by microscopy due to the diffraction limit. In this way, it is a more sensitive measure of small changes in turgor pressure needed for the pore to open. To elucidate the nature of noise in the resistance measurements, we have also performed DC electrical measurements that had limited effect (Fig. S7, ESI† Note S2), suggesting that the measurement noise comes from environmental disturbances.

After the first loss of contact, the resistance increased by 123 times, providing a sensor gain value, G. During the next cycles, G gradually decreased to 4 for the last closing. We note that sensor devices eventually fail (after 5–7 cycles) with a gradual loss of gain. The opening latency time (Fig. 2g) and the positions of the micropillars visible by microscopy remain invariant. Rather, apparently the electrical contact itself degrades over time accounting for the loss of gain. This suggests improvements in the composition of the ink or printed circuit can significantly extend the sensor lifetime. To show this, we varied the above fabrication method to replace the micropillars with thin conformal, polymer supported electrodes that were transferred and aligned onto stomata (see ESI† Note S4). Polymer stripes are initially applied, increasing the surface contact area of the conducting ink. On testing, these electrodes resulted in notably less electrical noise during measurements, but also increased opening latency time because of some overhang of the polymer supported electrodes in the pore.

Response to wavelength and fluence of incident light

To understand and predict stomatal opening and closing latencies, stomatal dynamics were experimentally studied under various illumination conditions *via* optical microscopy. There is a spectral dependence of the incident light on the stomatal aperture size (Fig. 3a). Both blue (400–500 nm) and red (600–700 nm) light can be absorbed by photosynthetic pigments present in guard cells, activating photophosphorylation of photoreceptors and activation of proton pumps in the stomatal guard cell plasma membrane.[37] Chloroplast carbon fixation leads to sucrose generation in the cytosol, increasing guard cells osmotic pressure and opening stomata.[38] Blue light also activates both phototropin 1 and phototropin 2 receptors, that transmit an activation signal to the plasma membrane H^+–ATPase.[29] H^+–ATPase activity hyperpolarizes the plasma membrane, leading to K^+, Cl^-, NO_3^-, and malate^{2-} uptake.[30] These ions also increase osmotic pressure, causing stomatal opening. This explains why blue light induces bigger stomatal openings as compared to red light, while a dual beam (red and blue) shows synergistic effect.[39] Guard cells osmotic pressure rises slowly compared to almost immediate change in chloroplast photosynthetic activity, leading to a gradual increase in the stomatal aperture.[40] For instance, when *Spathiphyllum* specimen is brought from dark into

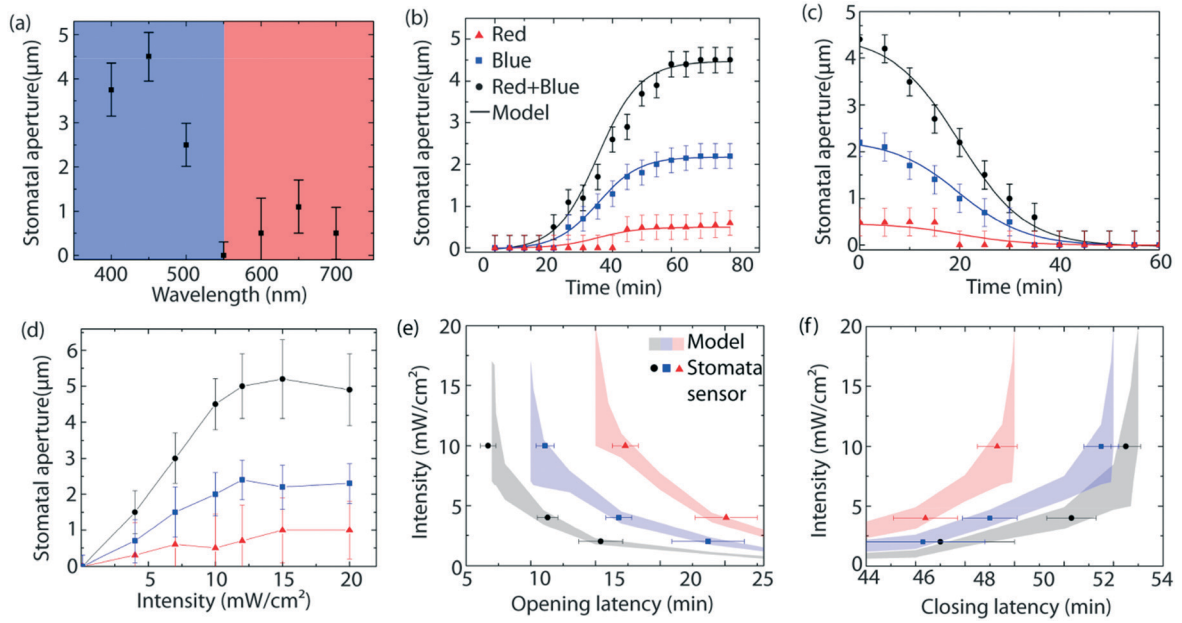

Fig. 3 *Spathiphyllum wallisii* stomatal response to visible light. (a) Optically measured stomatal aperture after illuminating the plant for 2 h with light of different wavelengths (I = 7 mW cm^{-2}, n = 3). (b) Stomatal opening dynamics (measured optically) in response to blue, red and dual lights (I = 10 mW cm^{-2}) illumination for the specimen kept in the dark beforehand. Points represent experimental measurements and lines – model fitting. (c) Same as (b), but shows stomata closing dynamics when the specimen is put in the dark after illuminating with different lights (I = 10 mW cm^{-2}). (d) Stomatal response to different light intensities for blue, red and dual lights after illuminating the plant for 2 h (n = 10). (e) Calculated and measured (n = 3) opening latency for various intensities of blue, red and dual lights. (f) Same as (e), but closing latency.

bright environment, their stomata open in the course of 60 min (Fig. 3b) and close within 30 min when the specimen is brought back into dark (Fig. 3c). Generally, stomata latency depends on the stomatal aperture across different species: smaller stomata typically have shorter response times.[15] As light intensity increases, the stomatal aperture first increases linearly and then saturates at white light 12 mW cm^{-2} (Fig. 3d). Note that large variations in stomata size measurements are caused by statistical differences (n = 10; aperture measurement error is 0.3 μm). This is associated with differences in rigidity of each pair of guard cells and pressure variations stemming from the neighboring cells.[17]

We find the opening latency to be 7.0 ± 0.5 min (Fig. 2g) upon illumination with white light I = 10 mW cm^{-2}, while the optical microscopy starts to resolve stomatal opening only 25 min after the illumination was turned on (Fig. 2e). To have access to stomatal dynamics below the diffraction limit, our experimental data (points in Fig. 3b) were compared with a mathematical model previously developed by Sun *et al.*[39] This model was created by synthesizing more than 85 articles on experimental observation of stomatal dynamics and signaling. It takes into account 70 different parameters described by discrete levels and more than 150 interactions between components that are implemented as the combination of logic and algebraic functions.[39] Since the experimental data on signaling pathway reaction speeds remains sparse, the model uses a random order asynchronous update rule. This mechanistic model successfully reproduces temporal dynamics as well as stomatal apertures under different illuminations (Fig. 3b and c). Following this success, we foresee that this model can be used to predict stomatal apertures under different conditions. For instance, in agriculture, this model will be useful to forecast effects of carbon dioxide, or the stress hormone abscisic acid (ABA; usually generated by plants during drought, salinity, pathogen attacks, UV radiation, and cold[41]). ABA initiates a biochemical pathway that ultimately inhibits the plasma membrane H^+–ATPase, closing stomata.[42] Furthermore, this model can distinguish contributions of ions to the total osmotic pressure in guard cells. This information can provide insights into fundamental research and identify possible knowledge gaps. Finally, this model can systematically compile and predict effects of single node knockouts.[39] Such capability opens ways for rapid testing of new phenotypes, saving time and resources for genetic engineering experiments.

The mechanistic model was further used to predict opening and closing latencies under different illuminations (the model differentiates blue and red lights that have different effect on stomata; following this, we used a lamp with 400–500 nm spectrum as the blue light source and a lamp with 600–700 nm spectrum as the red light source, see Methods). Comparing calculated stomatal dynamics (Fig. 3b and c) and electrical measurements (Fig. 2f), we found that resistance changes occur when the stomatal aperture becomes larger (smaller) than 10 nm when opening (closing). Using this information, latencies for various light intensities can be predicted (Fig. 3e and f). To estimate confidence intervals, we calculated the statistical error of latency measurements from Fig. 2g, and then graphically propagated this error into the intensity uncertainty (Fig. S8 and S9†). The results show good agreement between experimental measurements from the patterned stoma response and the mechanistic model. Furthermore, both opening and closing latencies differ significantly depending on light intensity and illumination conditions. Interestingly, the photodetector opening latency shows inverse sensitivity to light intensity, corresponding to an inverse sensor. This demonstrates that the sensor can distinguish light intensities up to 12 mW cm^{-2} with 1 mW cm^{-2} limit of detection, and light wavelength ranges incident upon the leaf, highlighting the use of latency as a predictive variable. Interestingly, variability in the stomatal aperture latency increases for smaller light intensities, consistent with an increasing effect of neighboring cells on the stomata (ESI† Note S3) unaccounted for in the model. This topic requires further study,[43,44] however, our work shows that *Spathiphyllum* stomata have strong collective behavior, which is revealed under non-uniform illumination (Fig. S16†).

Stomata and the diurnal cycle under drought

The sensor stability over several days allows it to be applied to time scales relevant for long term plant physiological processes. One example of this is drought detection. Drought, or abnormally long periods of low rainfall, reduces soil water potential, resulting in reduced agricultural productivity and ecosystem distortion. Generally, plants have drought tolerance mechanisms with cascaded structures.[9] In the case of mild drought conditions, plants withstand water shortage, regulating their transpiration rates through stomata. Persistent drought results in water conservation, stomatal closure, and decreased photosynthetic rates. Beyond this, oxidative damage cannot be suppressed.[9] Various tools for detecting plant drought utilize this cascaded response.[45] For example, genomic methods study changes in regulatory genes that are associated with photosynthesis, plant hormones, water and carbon dioxide management metabolic pathways. However, one of the major drawbacks is the difficulty in linking gene alternations with functional responses, as well as the labor needed. On the other hand, proteomic methods directly detect changes in various proteins (*e.g.*, ABA-responsive proteins, glycolysis proteins, membrane lignification) and associate their levels with water shortage, but are also labor intensive. Other techniques for drought detection (*e.g.*, isotope labeling, thermal and fluorescent imaging probes) have limited applicability.[45] As an alternative, stomatal apertures can function as the earliest and the quickest indicators of drought *via* two processes. When soil water potential drops, roots generate ABA in the plastidal 2-C-methyl-D-erythritol-4-phosphate pathway, which is then transported to leaf guard cells, inducing stomatal closure.[42] Also, guard cells lose water

and their turgor pressure decreases, increasing stomatal opening latency.

The stomatal aperture is tightly connected to illumination and therefore the natural diurnal cycle.[46] Our sensor successfully monitored the plant diurnal cycle of the stomatal aperture for 7 consecutive days (Fig. 4a). These measurements demonstrate resistance rise (drops) during light (dark) illumination conditions using a broadband incandescent emission source at 10 mW cm^{-2} corresponding to stomatal opening (closing). Similar to Fig. 2g, plant stomata had 7.0 ± 0.5 min opening latency and about 53.0 ± 0.5 min closing latency (Fig. 4b). Under normal conditions, plants were watered every 24 h. To simulate drought, watering was halted after the third day. Given the soil volume, water deficit becomes evident within 2 to 3 days, resulting in plant turgor pressure decrease that was observed visually (Fig. S10†). Soil water potential dropped from 5 to 62 kPa (Fig. 4c). During drought, stomatal opening latency gradually increased from 7.0 ± 0.5 to 25.0 ± 0.5 min; simultaneously, the closing latency decreased from 53.0 ± 0.5 to 45.0 ± 0.5 min. Optical microscopy of stomatal aperture response to light confirmed smaller stomatal apertures, increased opening latency, and decreased closing latency during drought (Fig. S21†). Payam *et al.* observed proteomic changes in multiple plant species during

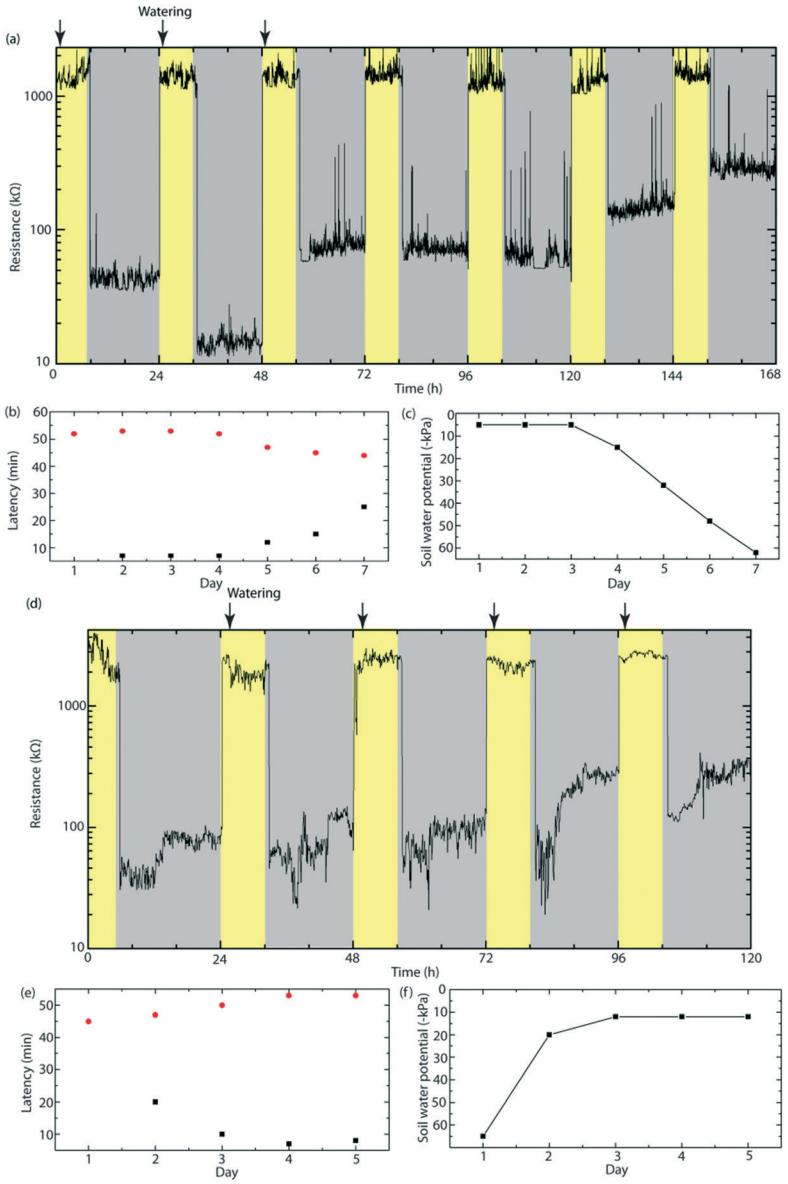

Fig. 4 SEMPSS monitors diurnal cycle in *Spathiphyllum wallisii*. (a) SEMPSS temporal resistance on a specimen during days (white light I = 10 mW cm^{-2}) and nights (yellow and grey boxes, respectively). The specimen was watered during the first three days. (b) Latencies for stomatal opening (black) and closing (red), extracted from (a), demonstrate stomatal retardation. Data points have 0.5 min error bars that are not visible. (c) Soil water potential, under conditions as in (a), shows drought onset. (d) Drought recovery experiment: a specimen was initially without water for four days. Watering started on the second day of the experiment. (e) Latencies for stomatal opening (black) and closing (red), extracted from (d), demonstrate gradual recovery after drought. (f) Soil water potential under conditions as in (d).

drought periods of 1–4 days.[47] In a separate experiment, we also studied plant recovery from a four day drought period (Fig. 4d; we have specifically chosen a stoma that showed a similar light response as the one used in the previous experiment). Initially, our microsensor reported the stomatal opening latency as 20.0 ± 0.5 min, and the closing latency – as 45.0 ± 0.5 min, corresponding to the retarded stomatal response observed in the previous experiment (Fig. 4e). After specimen watering on the second day, soil water potential gradually rose from 65 to 12 kPa and a stoma decreased (increased) its opening (closing) latency, stabilizing at 8.0 ± 0.5 min (53.0 ± 0.5 min) on the fifth day.

Conclusions

The microfluidic molding of a nanoparticle conducting ink directly across the stomata pore is shown to create a conductimetric interface to stomatal aperture. The resulting SEMPSS device is able to electrically differentiate open and closed states that are shown to correlate with the response of the plant to illumination and soil water status, providing a useful tool for the study of plant biology and its environment. The patterned stoma of *Spathiphyllum wallisii* acts as a living photodetector distinguishing fluences up to 12 mW cm^{-2}, differentiating between blue, red and white incident lights. Besides this, the microdetector is also used to assess plant drought response. To this end, a clear advantage of this approach is its persistence over extended monitoring periods, as we demonstrate for 7 days under conditions of decreasing soil water potential, without perturbing the plant environment. The opening latency of stomata was measured to change from 7.0 ± 0.5 min to 25.0 ± 0.5 min under such conditions. This sensor for single stomata aperture monitoring will improve our understanding of the endogenous and exogenous signals regulating stomatal aperture.[48,49] The method of non-destructive, biocompatible printing of conductive circuits directly onto the leaf with a micrometer precision may enable more complex electronic functions such as coupled radio-frequency identification, electrochemical and logic circuits. In this way, such circuits may enable the monitoring and engineering of novel plant functions.

Conflicts of interest

There are no conflicts to declare.

Acknowledgements

The authors acknowledge funding from the U.S. Department of Energy under contract 0000215305, Sime Darby, and Singapore-SMART program Disruptive Sustainable Technologies for Agricultural Precision (DISTAP). V. B. K. is supported by The Swiss National Science Foundation (projects no. P2ELP3_162149 and P300P2_174469). T. T. S. L. and M. H. W are both supported by the Agency of Science, Research and Technology Singapore. Microfabrication for this work was performed at the Harvard University Center for Nanoscale Systems (CNS), a member of the National Nanotechnology Coordinated Infrastructure Network (NNCI), which is supported by the National Science Foundation under NSF award no. 1541959. The authors wish to thank Southwest Nanotechnologies for the gift of AC100 sample, Dow corning for the gift of the adhesive kit, and G. Verma for helpful discussions.

References

1 M. M. Chaves, J. S. Pereira, J. Maroco, M. L. Rodrigues, C. P. P. Ricardo, M. L. OsÓRio, I. Carvalho, T. Faria and C. Pinheiro, *Ann. Bot.*, 2002, **89**, 907–916.
2 A. Fischlin, G. F. Midgley, J. T. Price, R. Leemans, B. Gopal, C. Turley, M. D. A. Rounsevell, O. P. Dube, J. Tarazona, A. A. Velichko, E. Publication and K. Brander, in *Climate Change 2007: Impacts, Adaptation and Vulnerability*, Contribution of Working Group II to the Fourth Assessment Report of the Intergovernmental Panel on Climate Change, Cambridge University Press, 2007, pp. 211–272.
3 M. M. Chaves, J. Maroco and J. Pereira, *Funct. Plant Biol.*, 2003, **30**, 239–264.
4 A. Nerd and P. S. Nobel, *Physiol. Plant.*, 1991, **81**, 495–500.
5 H. Nonami, *J. Plant Res.*, 1998, **111**, 373–382.
6 M. Farooq, A. Wahid, N. Kobayashi, D. Fujita and S. M. A. Basra, *Agron. Sustainable Dev.*, 2009, **29**, 185–212.
7 M. Hussain, M. A. Malik, M. Farooq, M. Y. Ashraf and M. A. Cheema, *J. Agron. Crop Sci.*, 2008, **194**, 193–199.
8 S. Munné-Bosch and J. Peñuelas, *Planta*, 2003, **217**, 758–766.
9 Z. Xu, G. Zhou and H. Shimizu, *Plant Signaling Behav.*, 2010, **5**, 649–654.
10 D. Wang, S. A. Heckathorn, X. Wang and S. M. Philpott, *Oecologia*, 2012, **169**, 1–13.
11 A. Herrera, *AoB Plants*, 2013, **5**, plt014.
12 L. Cheng, Y. Wang, Q. He, H. Li, X. Zhang and F. Zhang, *BMC Plant Biol.*, 2016, **16**, 188.
13 F. Morari, F. Meggio, A. Lunardon, E. Scudiero, C. Forestan, S. Farinati and S. Varotto, *Front. Recent Dev. Plant Sci.*, 2015, **6**, 314.
14 C. Willmer and M. Fricker, in *Stomata*, Springer, Netherlands, Dordrecht, 1996, pp. 354–365.
15 M. A. B. Camargo and R. A. Marenco, *Acta Amazonica*, 2011, **41**, 205–212.
16 L. Kappen, G. Andresen and R. Lösch, *J. Exp. Bot.*, 1987, **38**, 126–141.
17 M. Seo, D.-H. Park, C. W. Lee, J. Jaworski and J.-M. Kim, *Sci. Rep.*, 2016, **6**, 32394.
18 R. Zhu, S. M. Macfie and Z. Ding, *J. Exp. Bot.*, 2005, **56**, 2831–2838.
19 S. Hunt, *Physiol. Plant.*, 2003, **117**, 314–325.
20 C. Guo, Y. Yu and J. Liu, *J. Mater. Chem. B*, 2014, **2**, 5739–5745.
21 K. Lee, J. Park, M.-S. Lee, J. Kim, B. G. Hyun, D. J. Kang, K. Na, C. Y. Lee, F. Bien and J.-U. Park, *Nano Lett.*, 2014, **14**, 2647–2654.
22 I. Mouravieff, *Philos. Trans. R. Soc. London, Ser. B*, 1976, **273**, 561–564.
23 J. S. Moon, S. S. Lee, S. H. Lee and H. T. Kwon, *Microsyst. Technol.*, 2005, **11**, 311–318.

24 H. Kaiser and T. E. E. Grams, *J. Exp. Bot.*, 2006, **57**, 2087–2092.
25 J. L. Wilbur, A. Kumar, E. Kim and G. M. Whitesides, *Adv. Mater.*, 1994, **6**, 600–604.
26 H. Miyajima and M. Mehregany, *J. Microelectromech. Syst.*, 1995, **4**, 220–229.
27 K. Koch and W. Barthlott, *Philos. Trans. R. Soc., A*, 2009, **367**, 1487–1509.
28 I. Vanstechelman, H. Vansteenkiste, T. Eeckhaut, J. Van Huylenbroeck and M. C. Van Labeke, *Acta Hortic.*, 2009, **836**, 79–84.
29 K.-I. Shimazaki, M. Doi, S. M. Assmann and T. Kinoshita, *Annu. Rev. Plant Biol.*, 2007, **58**, 219–247.
30 S. M. Assmann, L. Simoncini and J. I. Schroeder, *Nature*, 1985, **318**, 285–287.
31 M. R. G. Roelfsema and R. Hedrich, *New Phytol.*, 2005, **167**, 665–691.
32 M. Amjadi, K.-U. Kyung, I. Park and M. Sitti, *Adv. Funct. Mater.*, 2016, **26**, 1678–1698.
33 K. Rajan, I. Roppolo, A. Chiappone, S. Bocchini, D. Perrone and A. Chiolerio, *Nanotechnol., Sci. Appl.*, 2016, **9**, 1–13.
34 J. P. Giraldo, M. P. Landry, S. M. Faltermeier, T. P. McNicholas, N. M. Iverson, A. A. Boghossian, N. F. Reuel, A. J. Hilmer, F. Sen, J. A. Brew and M. S. Strano, *Nat. Mater.*, 2014, **13**, 400–408.
35 M. H. Wong, J. P. Giraldo, S.-Y. Kwak, V. B. Koman, R. Sinclair, T. T. S. Lew, G. Bisker, P. Liu and M. S. Strano, *Nat. Mater.*, 2017, **16**, 264–272.
36 O. P. Parida and N. Bhat, *Int. Conf. Optics and Photonics*, 2009, s.3, p. 8.
37 A. Schwartz and E. Zeiger, *Planta*, 1984, **161**, 129–136.
38 A. R. Reddy and V. S. R. Das, *Plant Cell Physiol.*, 1986, **27**, 1565–1570.
39 Z. Sun, X. Jin, R. Albert and S. M. Assmann, *PLoS Comput. Biol.*, 2014, **10**, e1003930.
40 T. Lawson and M. R. Blatt, *Plant Physiol.*, 2014, **164**, 1556–1570.
41 R. Finkelstein, *The Arabidopsis Book*, 2013, p. e0166.
42 S. Gepstein, M. Jacobs and L. Taiz, *Plant Sci. Lett.*, 1982, **28**, 63–72.
43 A. Savvides, D. Fanourakis and W. van Leperen, *J. Exp. Bot.*, 2011, **63**(3), 1135–1143.
44 K. A. Mott and T. N. Buckley, *Trends Plant Sci.*, 2000, **5**, 258–262.
45 M. M. Chaves, J. P. Maroco and J. S. Pereira, *Funct. Plant Biol.*, 2003, **30**, 239–264.
46 C. Sánchez, G. Fischer and D. W. Sanjuanelo, *Agron. Colomb.*, 2013, **31**, 38–47.
47 M. Payam Pour, N. Mohammad-Zaman and K. Setsuko, *Curr. Proteomics*, 2012, **9**, 232–244.
48 K. A. Mott, D. G. Berg, S. M. Hunt and D. Peak, *Plant, Cell Environ.*, 2014, **37**, 1184–1191.
49 T. Lawson, A. J. Simkin, G. Kelly and D. Granot, *New Phytol.*, 2014, **203**, 1064–1081.

